E. coli translation strategies differ across nutrient conditions

Authors: Sophia Hsin-Jung Li[1], Zhiyuan Li[2], Junyoung O. Park[3,4], Christopher G. King[5], Joshua D. Rabinowitz[3,6], Ned S. Wingreen*[1,3], and Zemer Gitai*[1]

Affiliations:

[1]Department of Molecular Biology,

[2]Princeton Center for Theoretical Science,

[3]Lewis-Sigler Institute for Integrative Genomics,

[4]Department of Chemical and Biological Engineering,

[5]Department of Physics, and

[6]Department of Chemistry, Princeton University, Princeton, NJ, USA.

*Correspondence to: wingreen@princeton.edu, zgitai@princeton.edu

Abstract

For cells to grow faster they must increase their protein production rate. Microorganisms have traditionally been thought to accomplish this increase by producing more ribosomes to enhance protein synthesis capacity, leading to the linear relationship between ribosome level and growth rate observed under most growth conditions previously examined. Past studies have suggested that this linear relationship represents an optimal resource allocation strategy for each growth rate, independent of any specific nutrient state. Here we investigate protein production strategies in continuous cultures limited for carbon, nitrogen, and phosphate, which differentially impact substrate supply for protein versus nucleic acid metabolism. Unexpectedly, we find that at slow growth rates, *E. coli* achieves the same protein production rate using three different strategies under the three different nutrient limitations. Upon phosphate (P) limitation, translation is slow due to a particularly low abundance of ribosomes, which are RNA-rich and thus particularly costly for phosphorous-limited cells. In nitrogen (N) limitation, translation is slowed by limited glutamine and stalling at glutamine codons, resulting is slow elongation. In carbon (C) limitation, translation is slowed by accumulation of inactive ribosomes not bound to mRNA. These extra ribosomes enable rapid growth acceleration upon nutrient upshift. Thus, bacteria tune ribosome usage across different limiting nutrients to enable balanced nutrient-limited growth while also preparing for future nutrient upshifts.

Introduction

Resource allocation during growth is a fundamental challenge faced by all cells[1-4]. For example, with a fixed resource budget, cells must balance production of the machinery that makes proteins (ribosomes, tRNAs, translation factors) with the production of the proteins themselves. This balance is generally represented by the RNA:protein ratio (R/P ratio)[5]. The R/P ratio captures protein production capacity, as >95% of total RNA is devoted to translation (rRNAs and tRNAs[5,6]). In single-cell organisms like *E. coli*, previous studies demonstrated that

there is a linear relationship between R/P ratio and growth rate, with faster growth rates requiring more protein production capacity and therefore higher R/P ratios[5,7,8]. Production of ribosomes is costly as each contains 52 protein subunits and three large rRNAs[9,10]; hence, it is advantageous for the cell to saturate ribosomes with substrates. In this efficient ribosome scenario, the ribosome level should be fixed and independent of nutrient conditions for any growth rate, with the only way to increase protein synthesis rate being to increase the number of ribosomes[1,5,11]. One surprise for such a seemingly optimized system is that multiple studies have demonstrated that at slow growth rates *E. coli* accumulates inactive ribosomes[12]. There are two possible explanations for the presence of inactive ribosomes. First, it is possible that *E. coli* translation is constrained in such a way that it cannot function when ribosome levels drop too low[12]. Alternatively, *E. coli* could regulate ribosome production independently of growth rate. Here we settle this debate by showing that *E. coli* ribosome production and usage differ across nutrient conditions.

Results

Phosphate-limited cells achieve the same growth rate with fewer ribosomes than Carbon- or Nitrogen-limited cells

To determine the generality of the relationship between growth rate and ribosome content, we examined how the R/P ratio changes as a function of growth upon different nutrient limitations. We measured R/P ratios in *E. coli* under glucose- (C, carbon), ammonia- (N, nitrogen), and phosphate- (P, phosphorous) limitations over a range of different growth rates in chemostats (Figure 1A). Surprisingly, P-limited cells consistently exhibited lower R/P ratios than C-limited or N-limited cells, with a roughly 2-fold difference at the slowest growth rate tested (0.1 h^{-1}, Figure 1B). Measured protein levels were similar in all cells regardless of growth rate or nutrient limitation (Figure S1A-B), indicating that the changes in the R/P ratios reflect changes in ribosome availability.

The finding that *E. coli* can grow at the same rate with a lower R/P ratio implies that P-limited cells make the same amount of protein with fewer ribosomes, i.e. use ribosomes more efficiently. Thus, C/N-limited *E. coli* cells do not use ribosomes with optimal efficiency and their supply of "extra" ribosomes cannot be ascribed to requirements for productive translation. Since RNA accounts for two-thirds of the mass of bacterial ribosomes[9,14], producing fewer ribosomes upon phosphate-limitation makes sense as a way for cells to deal with a limitation that preferentially reduces an elemental substrate needed to make RNA but not protein. This effect may be a direct consequence of low phosphate resulting in limited nucleotide pools and thus slow RNA synthesis, as deletion of phosphate sensing or storage systems, phoB[15] or ppk[16], did not alter the R/P ratio (Figure S1C-D).

N-limited ribosomes translate slowly while C-limited cells accumulate more mRNA-free ribosomes

Why do C/N-limited cells accumulate so many ribosomes if P-limited cells can achieve the same protein synthesis rates with fewer ribosomes? One possibility is that the ribosomes in these cells translate slowly. We thus used a *lacZ* induction assay to compare the translation elongation rates of slow-growing C-, N-, and P-limited cells (0.1 h^{-1})[17,18]. We observed a reduced elongation rate in N-limited cells compared to C- and P-limited cells but no difference between C- and P-limited cells (Figure 1C). Thus, N-limited cells may need higher ribosome numbers to compensate for their slow translation elongation, but something else must explain the elevated ribosome numbers in C-limited cells.

To characterize ribosome pools we performed polysome profiling, which separates ribosome species using a sucrose gradient[19]. Regardless of the growth condition, all cells exhibited similar fractional pools of dissociated 30S and 50S subunits (Figure 1D). In contrast, the fraction of 70S monosomes was significantly larger in C/N-limited cells than in P-limited cells (Figure 1D). Since growth rate is proportional to protein synthesis rate, growth rate can be

91 estimated by the product of the number of active ribosomes and the translation elongation rate.
92 However, using the assumption that all 70S monosomes are active yielded very different growth
93 rate estimates for C-, N-, and P-limited cells (Figure 1F and SI), which is inconsistent with the
94 fact that these cells are growing at the same rate and have the same protein content. This
95 inconsistency suggested that a fraction of the 70S ribosomes may not be active.

96 The mass of a single mRNA is small relative to the mass of a ribosome, such that 70S
97 monosomes could represent either mRNAs with only one ribosome per transcript or inactive
98 "free" ribosomes that are not associated with an mRNA. To distinguish free and mRNA-bound
99 70S monosomes, we utilized their differential sensitivity to high potassium levels (170 mM)[20].
100 High potassium causes free ribosomes to shift to a lower density but does not shift the density
101 of mRNA-bound monosomes[20]. We thus designed a high-resolution "free-ribosome profiling"
102 method to resolve this density shift (Figure S2). As controls, we confirmed that our assay
103 detects the potassium-dependent shift of 70S monosomes induced by puromycin (Figure S2),
104 which releases elongating ribosomes from their associated mRNAs[21]. There was no potassium-
105 dependent shift detected in fast-growing cells that lack free ribosomes (Figure S2).

106 By combining traditional and free-ribosome polysome profiling, we quantified the relative
107 fractions of all ribosome species in slow-growing C-, N-, and P-limited *E. coli*. The fraction of
108 free monosomes was roughly 3-fold greater in the C-limited cells than in the P-limited cells,
109 while the fraction of mRNA-bound monosomes remained relatively constant across nutrient
110 limitations (Figure 1E). The accumulation of free 70S monosomes in C- and N-limited cells
111 appears to be independent of a previously-described RaiA-dependent mechanism for ribosome
112 storage as deletion of *raiA* had no impact on R/P ratios or polysome profiles (Figure S3).
113 Importantly, revising our protein synthesis rate estimates to account for the fraction of inactive
114 70S monosomes yielded similar values for all cells, regardless of nutrient limitation (Figure 1F).
115 These results both validate our experimental measurements and suggest that in different

116 nutrient states, *E. coli* differentially tune ribosome number, translation rate, and active fraction to
117 produce proteins at the same rates (Figure 2A).

118 ***Quantitative modeling describes three different strategies of ribosome dynamics to***
119 ***achieve the same protein production rate***

120 To better understand nutrient-dependent ribosome dynamics, we probed translation in
121 slow-growing C-, N-, and P-limited cells by ribosome profiling. Analysis of ribosome densities as
122 a function of distance from the start and stop codons revealed higher ribosome occupancy near
123 the start codon (Figure 2B). Ribosome density thereafter was similar, with no decrease in
124 ribosome density between the first and second halves of genes (Figures 2B and S4A),
125 suggesting that there is little to no aborted translation after the first few codons. We quantified
126 ribosome dynamics by building a simple macroscopic model (Figure 2C, S4B-E and details in
127 SI). In this model, unbound ribosomes (R_u) can bind to an mRNA with a free ribosomal binding
128 site (with rate constant k_f) to become initiating ribosomes (R_i). The initiating ribosomes can
129 proceed to elongation (with rate constant k_p) to become working ribosomes (R_w), or can abort
130 translation (with rate constant k_r). Working ribosomes elongate to finish translation and become
131 unbound (with rate constant k_{el}/N_{aa}), where N_{aa} is the length of an average protein in amino
132 acids. We defined the fraction of ribosomes bound to the first 10 codons as initiating ribosomes
133 since the ribosome footprint size is ~10 codons[22,23]. To validate our model we used it to
134 calculate elongation rates, which closely agreed with those we measured experimentally (Figure
135 S5A).

136 Analysis of our model indicated that the system can be characterized by two main
137 dimensionless parameters: the "relative proceeding rate", defined as the ratio between the rate
138 of ribosomes proceeding from initiation to elongation (k_p, s^{-1}) and the rate of elongation (k_{el}/N_{aa},
139 s^{-1}); and the "saturation parameter" ($R_t/(K_m+R_t)$), reflecting the degree of saturation of ribosome
140 binding sites on mRNAs, where R_t is the total ribosome number and $K_m = (k_r + k_p)/k_f$ (Figures

141 2D-E and S5B-C). Fitting the measured ribosome densities, translation elongation rates, and
142 pool sizes of ribosome species to the macroscopic model revealed that P-limited cells have the
143 highest relative proceeding rate while C-limited cells have the lowest saturation parameter, and
144 N-limited cells have intermediate values for both parameters (Figures 2D-E and S5B-H). Thus,
145 C-, N-, and P-limited cells produce proteins at the same rate using three different strategies: P-
146 limited cells have few ribosomes that are mostly active and elongate rapidly, N-limited cells
147 have more ribosomes but fewer are active and they elongate slowly, and C-limited cells have
148 many ribosomes, which elongate rapidly, but even fewer are bound to mRNA (Figure 2F and
149 S5I).

150 ***N-limited ribosomal regulation is mediated by RelA, the ppGpp alarmone synthase***

151 Insight into the molecular basis of nutrient-specific ribosome regulation came from
152 analysis of the codon occupancies in our ribosome profiling data. Codon-specific ribosome
153 stalling leads to increased codon occupancy and is a hallmark of insufficient pools of the
154 corresponding charged tRNAs. P-limited cells exhibited no elevated codon frequencies,
155 consistent with these cells' efficient ribosome usage (Figure 3A). In contrast, both C- and N-
156 limited cells exhibited significant codon-specific stalling. Under N-limitation, ribosomes stalled at
157 both of the two glutamine-encoding codons, which together account for 4.4% of all predicted
158 ORF codons in *E. coli*. This result is consistent with previous studies indicating that glutamine is
159 the most strongly-depleted amino acid pool upon N-limitation and serves as an intracellular
160 sensor for extracellular nitrogen levels[24-26]. Upon C-limitation, we observed elevated occupancy
161 of the Leu-CUA codon, which was surprising as there is no known intracellular carbon sensor
162 that controls translation. *E. coli* has six leucine codons decoded by five leucine tRNA
163 species[27,28]. Leu-CUA is the rarest Leu codon, accounting for only 0.4% of all predicted ORF
164 codons.

165 In addition to clarifying the link between metabolism and translation for N-limitation, the
166 observation that ribosomes stall at specific codons upon C/N-limitation suggested a molecular
167 mechanism for nutrient-specific translation regulation (Figure 3A). In bacteria, insufficient
168 charged tRNA pools activate the stringent response to induce accumulation of the cellular
169 alarmone, ppGpp[30,31]. ppGpp is known to regulate rRNA transcription *in vivo*. Its role in
170 translation is less well-understood but ppGpp has been shown *in vitro* to inhibit translation
171 factors such as EF-Tu and IF2 by competing with GTP[32,33]. To test how ppGpp accumulation
172 might affect translation *in vivo*, we induced ppGpp synthesis by treating batch-grown *E. coli* with
173 serine hydroxamate (SHX). SHX is a serine analog that competitively inhibits serine tRNA
174 synthetase to yield uncharged serine-tRNA and thereby activate the RelA ppGpp synthase[34].
175 SHX treatment increased the pool of mRNA-free 70S monosomes, and this effect was
176 completely dependent on *relA* (Figures S6A-B). Thus, inducing ppGpp by activating RelA alters
177 translation by increasing the fraction of inactive free 70S ribosomes.

178 RelA is primarily required for the accumulation of ppGpp upon N-limitation but not C-
179 limitation[31]. Consistently, deletion of *relA* had little impact on the accumulation of free ribosomes
180 upon C-limitation, but significantly reduced free ribosome pools upon N-limitation to levels
181 similar to those observed upon P-limitation (Figures 3B and S6C). We could not probe the role
182 of ppGpp in C-limited ribosome accumulation because unlike N-limitation, C-limitation elevates
183 ppGpp through *spoT*, which is essential[35]. N-limited *ΔrelA* cells also contained more polysomes
184 than wild type (Figure 3B), suggesting that these cells had a higher fraction of elongating
185 ribosomes. This result was initially confusing because the wild type and *ΔrelA* N-limited cells
186 were grown at the same growth rate and maintained the same R/P ratio (Figure S6D). We thus
187 measured the rate of translation elongation and found that while N-limited *ΔrelA* cells have
188 higher fractions of translating ribosomes, their ribosomes elongate more slowly (Figure 3C),
189 resulting in the same rate of protein production as wild type.

190 To understand how RelA influences ribosome dynamics we performed ribosome
191 profiling. N-limited *ΔrelA* cells exhibited more pronounced ribosome stalling at both glutamine
192 codons than wild type N-limited cells, while *relA* deletion had no effect on P- or C-limited cells
193 (Figures 3D and S7). Fitting the *ΔrelA* cells measurements to our ribosome dynamics model
194 revealed that *ΔrelA* cells specifically increase the relative proceeding rate under N-limitation, but
195 display no effect on relative proceeding rate under P- or C-limitation and no effect on the
196 saturation parameter in any condition (Figures 3E and S5B-C). These results suggest that,
197 consistent with its known effects on IF-2 *in vitro*, in N-limited cells RelA functions to restrict the
198 transition from translational initiation to elongation. Thus, in the absence of RelA, more
199 ribosomes attempt to elongate, which exacerbates the depletion of charged tRNA pools, leading
200 to increased stalling and a slower translational elongation rate.

201 ***Extra ribosomes may facilitate growth acceleration upon nutrient upshift***

202 While cells can modulate different aspects of ribosome dynamics to achieve the same
203 protein production rate, what benefits might be served by the inefficient translation system used
204 by C-limited cells where many ribosomes are inactive? Since free ribosomes accumulate the
205 most at the slowest growth rates, we hypothesized that our findings could reflect a trade-off
206 between steady-state growth rate and the ability to respond to a fluctuating environment. Such
207 transitions could include rapidly and safely slowing growth when nutrients become depleted and
208 rapidly increasing growth rate when nutrients are replenished. In this scenario, cells may benefit
209 more by optimizing their ability to rapidly utilize new nutrients, for example to outcompete their
210 neighbors or maximally utilize a transient pulse of nutrients, than by optimizing steady-state
211 growth rate when nutrient levels are low.

212 We built a mathematical model of cellular resource allocation to predict the growth
213 dynamics upon upshift. This model supported the hypothesis that the larger free ribosome pools
214 of C/N-limited cells should enable them to increase their growth rates more quickly than P-

215 limited cells upon nutrient upshift (Figures 4A, S8 and details in SI)[4,36]. We experimentally tested
216 this prediction by measuring the growth rates of slow-growing (0.1 h^{-1}) *E. coli* immediately after
217 being shifted to rich media (LB + 0.4% glucose) [37]. As predicted, C/N-limited cells increased
218 their growth rates significantly faster than P-limited cells (Figure 4B). Thus, the distinct
219 translation strategies employed under different nutrient conditions may represent nutrient-
220 specific adaptations, with P-limited cells optimizing for current steady-state growth under slow
221 growth conditions, and C- and N-limited cells favoring the ability to rapidly recover growth
222 (Figure 4C).

223 **Discussion**

224 In previous studies, *E. coli* were found to vary R/P ratio with growth rate independently of
225 the specific nutrient limitation used to produce a given growth rate[5,8]. Meanwhile, transcriptional
226 analysis in *Saccharomyces cerevisiae* suggested that the primary determinant of the response
227 to a wide range of stresses was the cellular growth rate rather than the specific stressor[38].
228 Together, these studies suggested that the primary regulator of microbial physiology is growth
229 rate. However, our findings demonstrate that at the same growth rate, *E. coli* exhibit significantly
230 different translation strategies across nutrient limitations; at the lowest growth rate tested, P-
231 limited cells produced the same amount of protein with roughly half as many ribosomes as C/N-
232 limited cells. P-limited cells also exhibited smaller inactive 70S monosome pools and higher
233 relative proceeding rates than C/N-limited cells. Furthermore, while C/N-limited cells have
234 similar ribosome numbers, they also display differences in free ribosome pools, translational
235 elongation rates, and sensitivity to the loss of the ppGpp synthase RelA. Thus, our results
236 suggest that the extra ribosomes of C/N-limited cells do not reflect essential constraints, but
237 rather reflect a selectively beneficial adaptation.

238 Our findings also implicate ppGpp as a key mediator of ribosome activity that specifically
239 modulates the transition from translation initiation to elongation. ppGpp is a well-characterized

240 cellular alarmone that senses translational activity and inhibits rRNA transcription[31,39]. However,
241 ppGpp can competitively inhibit GTP-dependent enzymes, including the translation initiation
242 factor IF-2 that is required for the transition to elongation[40]. Our data thus provide *in vivo* support
243 for a previous *in vitro* study demonstrating that ppGpp inhibits IF-2 function[33]. Since ppGpp can
244 also affect other GTP-binding proteins involved in translation[32,41], future studies on bacterial
245 translation will confirm exactly how ppGpp interferes with ribosome function.

246 In native environments such as the mammalian gut, bacteria such as *E. coli* are faced
247 with feast and famine cycles induced by feeding cycles[42]. Here we show that the linear
248 relationship between R/P ratio and growth rate in *E. coli* does not reflect the optimization of
249 steady-state growth rate but, instead, reflects the ability of cells with higher inactive ribosome
250 pools to rapidly accelerate growth upon nutrient repletion. These findings suggest that *E. coli*
251 may improve their fitness by sacrificing their maximal growth rate in nutrient-poor periods in
252 return for the ability to respond to a changing environment, including rapidly accelerating growth
253 in nutrient-rich periods. Our macroscopic model highlights how cells can tune total ribosome
254 number, the fraction of working ribosomes, and the rate of translational elongation to achieve
255 the same total protein production rate while balancing other constraints such as reduced amino
256 acid availability or the need to rapidly accelerate growth. Future studies will address the
257 consequences of adaptation strategies in dynamic conditions, for example the generality of
258 bacteria optimizing growth rate transitions at the expense of steady-state growth[43], but this
259 strategy could explain recent reports of the sub-optimality of protein allocation for *E. coli* in the
260 presence of poor carbon sources[44], as well as the sub-optimal expression levels of essential
261 genes in *B. subtilis*[45].

262

263 **Author Contributions**

264 S.H.L., J.O.P., J.D.R., N.S.W, and Z.G. designed the experiments. S.H.L., J.O.P., and C.K.
265 performed experiments. Z.L. and N.S.W. constructed the mathematical models. S.H.L.

conducted computational analysis of sequencing data. S.H.L, Z.L., N.S.W, and Z.G. wrote the paper with assistance from J.D.R.

Acknowledgments:

We thank the members of the Gitai, Wingreen, and Rabinowitz labs for helpful discussions. We thank Gene-Wei Li for his support for the ribosome profiling experiments. We thank the Microarray Core Facility at the Lewis-Sigler Institute (Daniel Sanchez, Jennifer M. Miller, Jessica Wiggins, and Wei Wang) for RNA-Seq sample processing and sequencing and the Princeton Proteomics Core Facility (Henry Shwe and Tharan Srikumar) for ribosome profiling sample processing. Lance Parsons provided helpful technical support for bioinformatics analysis of the sequencing data. We thank the Botstein lab, particularly Sandy Silverman, for chemostat operation support and all former members for discussions relating to microbial growth.

The ribosome sequencing data that support the findings of this paper will be deposited in GenBank with the accession code at publication.

This work was supported by grants from the NIH (DP1AI124669 and R01GM082938).

References and Notes:

1. You, C. *et al.* Coordination of bacterial proteome with metabolism by cyclic AMP signalling. **500,** 301–306 (2013).
2. Li, G.-W., Burkhardt, D., Gross, C. & Weissman, J. S. Quantifying absolute protein synthesis rates reveals principles underlying allocation of cellular resources. *Cell* **157,** 624–635 (2014).
3. Scott, M., Klumpp, S., Mateescu, E. M. & Hwa, T. Emergence of robust growth laws from optimal regulation of ribosome synthesis. *Mol. Syst. Biol.* **10,** 747–747 (2014).
4. Giordano, N., Mairet, F., Gouzé, J.-L., Geiselmann, J. & de Jong, H. Dynamical Allocation of Cellular Resources as an Optimal Control Problem: Novel Insights into Microbial Growth Strategies. *PLoS Comput. Biol.* **12,** e1004802 (2016).
5. Bremer, H. & Dennis, P. P. Modulation of Chemical Composition and Other Parameters of the Cell at Different Exponential Growth Rates. *EcoSal* 1–56 (2012).
6. Baracchini, E. & Bremer, H. Determination of synthesis rate and lifetime of bacterial mRNAs. *Anal. Biochem.* **167,** 245–260 (1987).
7. Schaechter, M., Maaløe, O. & Kjeldgaard, N. O. Dependency on Medium and Temperature of Cell Size and Chemical Composition during Balanced Growth of Salmonella typhimurium. *Microbiology* **19,** 592–606 (1958).
8. Scott, M., Gunderson, C. W., Mateescu, E. M., Zhang, Z. & Hwa, T. Interdependence of cell growth and gene expression: origins and consequences. *Science* **330,** 1099–1102 (2010).
9. Yamamoto, T., Izumi, S. & Gekko, K. Mass spectrometry of hydrogen/deuterium exchange in 70S ribosomal proteins from E. coli. *FEBS Lett.* **580,** 3638–3642 (2006).
10. Nomura, M. & Gourse, R. Regulation of the synthesis of ribosomes and ribosomal components. *Annual review of …* (1984).
11. Maaløe, O. & Kjeldgaard, N. O. *Control of Macromolecular Synthesis, WA Beniamin*. (Inc., 1966).

12. Dai, X. *et al.* Reduction of translating ribosomes enables Escherichia coli to maintain elongation rates during slow growth. *Nat Microbiol* **2,** 16231 (2016).
13. Klumpp, S., Scott, M., Pedersen, S. & Hwa, T. Molecular crowding limits translation and cell growth. *Proc. Natl. Acad. Sci. U.S.A.* **110,** 16754–16759 (2013).
14. Lewin, B. *Genes VIII*. (Pearson education, Inc, 2003).
15. Wanner, B. L. Gene regulation by phosphate in enteric bacteria. *Journal of Cellular Biochemistry* **51,** 47–54 (1993).
16. Ahn, K. & Kornberg, A. Polyphosphate kinase from Escherichia coli. Purification and demonstration of a phosphoenzyme intermediate. *J. Biol. Chem.* **265,** 11734–11739 (1990).
17. Schleif, R., Hess, W., Finkelstein, S. & Ellis, D. Induction kinetics of the L-arabinose operon of Escherichia coli. *J. Bacteriol.* **115,** 9–14 (1973).
18. Dalbow, D. G. & Young, R. Synthesis time of β-galactosidase in Escherichia coli B/r as a function of growth rate. *Biochemical Journal* **150,** 13–20 (1975).
19. Qin, D. & Fredrick, K. Analysis of polysomes from bacteria. *Meth. Enzymol.* **530,** 159–172 (2013).
20. Beller, R. J. & Lubsen, N. H. Effect of polypeptide chain length on dissociation of ribosomal complexes. *Biochemistry* **11,** 3271–3276 (1972).
21. Nathans, D. Puromycin inhibition of protein synthesis: incorporation of puromycin into peptide chains. *Proc. Natl. Acad. Sci. U.S.A.* **51,** 585–592 (1964).
22. Steitz, J. A. Polypeptide Chain Initiation: Nucleotide Sequences of the Three Ribosomal Binding Sites in Bacteriophage R17 RNA. **224,** 957–964 (1969).
23. Ingolia, N. T., Ghaemmaghami, S., Newman, J. R. S. & Weissman, J. S. Genome-wide analysis in vivo of translation with nucleotide resolution using ribosome profiling. *Science* **324,** 218–223 (2009).
24. Doucette, C. D., Schwab, D. J., Wingreen, N. S. & Rabinowitz, J. D. α-Ketoglutarate coordinates carbon and nitrogen utilization via enzyme I inhibition. *Nature Chemical Biology* **7,** 894–901 (2011).
25. Yuan, J. *et al.* Metabolomics-driven quantitative analysis of ammonia assimilation in E. coli. *Mol. Syst. Biol.* **5,** 302 (2009).
26. Ikeda, T. P., Shauger, A. E. & Kustu, S. Salmonella typhimuriumApparently Perceives External Nitrogen Limitation as Internal Glutamine Limitation. *Journal of Molecular Biology* **259,** 589–607 (1996).
27. Subramaniam, A. R., Pan, T. & Cluzel, P. Environmental perturbations lift the degeneracy of the genetic code to regulate protein levels in bacteria. *Proc. Natl. Acad. Sci. U.S.A.* **110,** 2419–2424 (2013).
28. Sørensen, M. A. *et al.* Over Expression of a tRNALeu Isoacceptor Changes Charging Pattern of Leucine tRNAs and Reveals New Codon Reading. *Journal of Molecular Biology* **354,** 16–24 (2005).
29. Elf, J., Nilsson, D., Tenson, T. & Ehrenberg, M. Selective charging of tRNA isoacceptors explains patterns of codon usage. *Science* **300,** 1718–1722 (2003).
30. Hauryliuk, V., Atkinson, G. C., Murakami, K. S., Tenson, T. & Gerdes, K. Recent functional insights into the role of (p)ppGpp in bacterial physiology. *Nat Rev Micro* **13,** 298–309 (2015).
31. Potrykus, K. & Cashel, M. (p)ppGpp: Still Magical? *. *Annu. Rev. Microbiol.* **62,** 35–51 (2008).
32. Mitkevich, V. A. *et al.* Thermodynamic characterization of ppGpp binding to EF-G or IF2 and of initiator tRNA binding to free IF2 in the presence of GDP, GTP, or ppGpp. *Journal of Molecular Biology* **402,** 838–846 (2010).
33. Milon, P. *et al.* The nucleotide-binding site of bacterial translation initiation factor 2 (IF2) as a metabolic sensor. *Proc. Natl. Acad. Sci. U.S.A.* **103,** 13962–13967

(2006).
34. Jiang, M., Sullivan, S. M., Wout, P. K. & Maddock, J. R. G-protein control of the ribosome-associated stress response protein SpoT. *J. Bacteriol.* **189,** 6140–6147 (2007).
35. Gentry, D. R. & Cashel, M. Mutational analysis of the Escherichia coli spoT gene identifies distinct but overlapping regions involved in ppGpp synthesis and degradation. *Mol. Microbiol.* **19,** 1373–1384 (1996).
36. Pavlov, M. Y. & Ehrenberg, M. Optimal control of gene expression for fast proteome adaptation to environmental change. *Proc. Natl. Acad. Sci. U.S.A.* **110,** 20527–20532 (2013).
37. Kjeldgaard, N. O., Maaløe, O. & Schaechter, M. The Transition Between Different Physiological States During Balanced Growth of Salmonella typhimurium. *Microbiology* **19,** 607–616 (1958).
38. Brauer, M. J. *et al.* Coordination of growth rate, cell cycle, stress response, and metabolic activity in yeast. *Mol. Biol. Cell* **19,** 352–367 (2008).
39. Paul, B. J., Ross, W., Gaal, T. & Gourse, R. L. rRNA Transcription in Escherichia coli. *Annu. Rev. Genet.* **38,** 749–770 (2004).
40. Laursen, B. S., Sørensen, H. P., Mortensen, K. K. & Sperling-Petersen, H. U. Initiation of protein synthesis in bacteria. *Microbiology and Molecular Biology Reviews* **69,** 101–123 (2005).
41. Rojas, A.-M., Ehrenberg, M. N., Andersson, S. G. E. & Kurland, C. G. ppGpp inhibition of elongation factors Tu, G and Ts during polypeptide synthesis. *Mol. Gen. Genet.* **197,** 36–45 (1984).
42. Zarrinpar, A., Chaix, A., Yooseph, S. & Panda, S. Diet and Feeding Pattern Affect the Diurnal Dynamics of the Gut Microbiome. *Cell Metabolism* **20,** 1006–1017 (2014).
43. Fischer, E. & Sauer, U. Large-scale in vivo flux analysis shows rigidity and suboptimal performance of Bacillus subtilis metabolism. *Nat. Genet.* **37,** 636–640 (2005).
44. Towbin, B. D. *et al.* Optimality and sub-optimality in a bacterial growth law. *Nat Commun* **8,** 14123 (2017).
45. Peters, J. M. *et al.* A Comprehensive, CRISPR-based Functional Analysis of Essential Genes in Bacteria. *Cell* **165,** 1493–1506 (2016).
46. Baba, T. *et al.* Construction of Escherichia coli K-12 in-frame, single-gene knockout mutants: the Keio collection. *Mol. Syst. Biol.* **2,** 2006.0008 (2006).
47. Zhu, M., Dai, X. & Wang, Y.-P. Real time determination of bacterial in vivoribosome translation elongation speed based on LacZα complementation system. *Nucleic Acids Res.* gkw698 (2016). doi:10.1093/nar/gkw698
48. Dunn, J. G. & Weissman, J. S. Plastid: nucleotide-resolution analysis of next-generation sequencing and genomics data. *BMC Genomics* **17,** 958 (2016).
49. Woolstenhulme, C. J., Guydosh, N. R., Green, R. & Buskirk, A. R. High-precision analysis of translational pausing by ribosome profiling in bacteria lacking EFP. *Cell Rep* **11,** 13–21 (2015).

Materials and Methods

Cell strains and growth conditions

Escherichia coli strain NCM3722 was grown in batch or continuous cultures. To achieve different growth rates, different carbon or nitrogen sources were provided in batch culture, whereas dilution rates ranging from 0.1 h^{-1} to 0.7 h^{-1} were used in continuous (chemostat)

412 cultures. The chemostat (Sixfors, HT) volume was 300mL with oxygen and pH probes to
413 monitor the culture. pH was maintained at 7.2 +/- 0.1 and the aeration rate was set at 4.5 l/h. 40
414 mM MOPS media (M2120, Teknova) was used with glucose (0.4%, Sigma G8270), ammonia
415 (9.5 mM NH_4Cl, Sigma A9434) and phosphate (1.32 mM K_2HPO_4, Sigma P3786) added
416 separately. For carbon- and nitrogen- limiting media, glucose and ammonia concentrations were
417 reduced by 5-fold (0.08% and 1.9mM respectively). Phosphorus-limiting medium contains 0.132
418 mM K_2HPO_4. Δ*relA* mutant was generated by P1 transduction from the KEIO collection[46] into
419 *Escherichia coli* strain NCM3722
420
421 Nutrient upshift growth measurement
422 Cells from chemosats were mixed with 4X volumes of fresh pre-warmed media and grown
423 in flasks in a 37°C water bath. Cell growth was monitored every 5 minutes by checking
424 absorbance at 600nm in a quartz cuvette (Starna, 16.160-Q-10/Z8.5) using a
425 spectrophotometer (GENESYS™ 20, Thermo Scientific). The LB media (244610, BD) used for
426 upshift was supplemented with 0.4% glucose.
427
428 Total RNA measurement
429 The method for RNA measurement was adapted from You *et al.*[1]. 1.5 mL of cultures were
430 pelleted by centrifugation for 1 min at 13,000 X g. The pellet was frozen on dry ice and the
431 supernatant was taken to measure absorbance at 600 nm for cell loss. The pellet was then
432 washed twice with 0.6M $HClO_4$ and digested with 0.3M KOH for 1 hour at 37˚C. The solution
433 was then precipitated with 3M $HClO_4$ and the supernatant was collected. The pellet was re-
434 extracted again with 0.5M $HClO_4$. The supernatants were combined and absorbance measured
435 at 260nm using NanoDrop (ND-1000, NanoDrop). Total RNA concentration was determined by
436 multiplying the A260 absorbance with 31 (µg RNA/mL) as the extinction coefficient.
437
438 Total protein measurement
439 The method for protein measurement is adapted from You *et al.*[1]. 1.5 mL of cell cultures were
440 pelleted by centrifugation for 1 min at 13,000 X g. Cells were washed with 1 mL MOPS buffer
441 once, re-suspended in 200 uL water and left on dry ice. All the supernatant was collected and
442 OD600 was measured for cell loss. To measure the protein content, samples were thawed,
443 100µL 3M NaOH were added, and the sample was heated for 5 min at 98˚C. The samples were
444 cooled down to RT for 5 min before 300µL 0.1% $CuSO_4$ were added for biuret assay. The
445 samples were incubated at RT for 5 min and centrifuged at 13,000 X g for 1 min. The
446 supernatant was collected and absorbance was measured at 555nm for a 200µL sample
447 volume in a microplate reader (Synergy HT, BioTek) with software Gen 5.0. Proper dilution of
448 albumin (23209, Thermo) with known concentrations was used to infer the total protein
449 concentration in the cell.
450
451 Polysome profiling and quantification of ribosome fraction
452 200mL of cells were collected from cultures by filtration through 90mm cellulose acetate
453 membranes with a 0.2 µm pore size (CA029025, Strelitech) at 37˚C, scratched with a clean and
454 pre-warmed stainless steel spatula, and snap-frozen in liquid nitrogen. The whole filtration
455 procedure did not take more than 2 minutes in order to maintain the original physiological state.
456 Cell pellets were mixed with 650µL lysis buffer frozen nuggets (20mM Tris-HCl pH 8.0, 10mM
457 $MgCl_2$, 100mM NH_4Cl, 0.4% Triton X-100, 0.1% NP-40, 1 mM Chloramphenicol, 100 U/mL
458 RNase-free DNase I (04716728001 Roche)) in a pre-chilled 10mL jar (014620331, Retsch).
459 Pulverization was done by cryomill (Retsch) at 15 Hz for 15 minutes. The thawed cell lysates
460 were quantified by NanoDrop and 200µL of lysates with RNA concentration ranging from 80µg
461 to 500µg were used. For overall polysome quantification, lysates were loaded to 10%-55%
462 linear sucrose gradients (20mM Tris-HCl pH 8.0, 10mM $MgCl_2$, 100mM NH_4Cl, 300 µM

463 Chloramphenicol) made by GradientMaster (BioComp). The gradients were placed in a SW41Ti
464 bucket and centrifuged in Optima XE-100 Ultracentrifuge (Beckman Coulter) at 35,000 rpm for 2
465 hours at 4˚C. Gradients were fractionated by BioComp Gradient Fractionator and the absorption
466 curves at 254nm were recorded by a UV monitor (EM-1, BioRad).
467 Quantification of the polysome profiles was done using customized MATLAB codes. First,
468 baselines were estimated using the readings where no peaks existed and the background was
469 subtracted. The background from the free nucleotides and tRNA was removed by fitting an
470 exponential decay function to the first peak representing the source of non-ribosome signals.
471 Each ribosome peak was picked and quantified by integrating the area underneath the curve.
472 To quantify different species of ribosomes in the 70S peak, 100mM NH_4Cl was replaced with
473 170mM KCl. Cell lysates were loaded onto 10%-30% linear gradient and centrifuged at 35,000
474 rpm at 4˚C for 5 h. Because the two peaks for the free and mRNA-bound 70S ribosomes are
475 very close in mass and clean separation was not possible, the MATLAB file-exchange package,
476 *peakfit*, was used to fit the two overlapped peaks as two Gaussian distributions. For the free
477 ribosome control, cells were treated with 100μM puromycin for 5 minutes and collected. For
478 serine hydroxamate (SHX, Sigma S4503) treatment, cells were grown in MOPS glucose
479 minimal media until OD ~0.3 and treated with SHX with final concentration of 1 mg/mL for ten
480 minutes before collection.
481
482 *lacZ* induction and translational elongation rate measurement
483 The method was adapted from Zhu et al[47]. A final concentration of 5 mM IPTG (I2481C-25,
484 Gold Biotechnology) was added to cultures. At every 15 seconds, 1 mL of culture was collected
485 in a tube containing 10μL 100mM chloramphenicol, snap frozen in liquid nitrogen and stored at -
486 20˚C before subsequent measurement. After cells were thawed, 400μL of the sample was
487 added to 100 μL 5x Z-buffer (0.3M $Na_2HPO_4.7H_2O$, 0.2M $NaH_2PO_4.H_2O$, 50mM KCl, 5mM
488 $MgSO_4$, 20mM β-mercaptoethanol) and incubated at 37˚C for 10 minutes. 100μL of 4mg/mL
489 MUG (337210010, ACROS Organics) in DMSO was then added to each sample every 10
490 seconds to accurately control the reaction time. The samples were incubated at 37˚C in a
491 thermomixer at 1,400 rpm mixing rate for 30 minutes to 2 hours, depending on the enzyme
492 expression level. The reaction was stopped by addition of 300μL of 1M Na_2CO_3. The tubes were
493 spun down at 16,000 X g for 3 minutes to sediment the cell debris. 200 μL of supernatant were
494 taken and measured fluorescence by a microplate reader (365 nm excitation and 450 nm
495 emission filter).
496 To infer translational elongation rate, the square root of the signal in excess of the signal at
497 time zero was plotted. A linear fit was performed on the points after signal began to increase.
498 The lag time is the x-intercept of the line. A previous study has shown that the initiation time
499 remains constant for about 10 seconds across a wide range of conditions tested[47]. Therefore,
500 we corrected the elongation times measured by subtracting 10 seconds in the lag times
501 measured.
502
503 Ribosome footprinting and total RNA extraction for RNA-Seq
504 The cell collection step was the same as for polysome profiling except that 1mM
505 chloramphenicol was used in the sucrose solution. The footprinting and library preparation steps
506 were adapted from Li *et al.*[2] After quantification of RNA concentration with NanoDrop, samples
507 with 500μg RNA were digested with 750U MNase (10107921001, Roche) for 1 hour at 25˚C
508 before being quenched with 6mM EGTA. The lysates were then layered onto a 10%-55%
509 sucrose gradient and centrifuged. The monosome fraction was collected and snap frozen in
510 liquid nitrogen. No polysome peaks were observed, indicating a thorough digestion. The RNA
511 was isolated using hot phenol and size selected on 15% TBE-Urea PAGE gels run for 1 hour at
512 210V. Gels were stained with SYBR Gold and visualized using Dark Reader (Clare Chemical
513 Research). RNA fragments with size between 25-40 nt were extracted using isopropanol

514 precipitation. Total RNA was extracted with TRIZOL from the same pulverized cells used for
515 footprinting. After DNaseI (04716728001,Roche) treatment and cleanup using RNA clean &
516 concentrator 5 (R1016, Zymo Research), ribosomal RNA was subtracted using MicrobeExpress
517 (AM1905, Ambion). The recovered RNA was fragmented and size selected. RNA fragments
518 with size between 25-40nt were extracted using isopropanol precipitation.
519
520 Library preparation and sequencing
521 Fragments from footprints and total RNA were dephosphorylated at the 3' end by PNK
522 (M0201, NEB). The repaired fragments were linked to the Universal miRNA Cloning Linker
523 (S1315S, NEB), reverse transcribed (18080044, Thermo)and circularized (CL4111K, Epicentre).
524 The circularized samples were PCR amplified (M0531L, NEB) and size selected. High quality
525 PCR samples checked by Bioanalyzer high sensitive DNA chip. Deep sequencing was done by
526 Illumina HiSeq 2500 on Rapid flowcells with settings of single end and 75 nt-long read length.
527
528 Mapping and sequencing data analysis
529 Data manipulation including barcode splitting, linker trimming and mapping were done
530 using Galaxy. The processed reads were mapped to *Escherichia coli* genome
531 escherichia_coli_k12_nc_000913_3 from the NCBI database with the BWA short read mapping
532 algorithm. Only the reads between 20-45 nt that aligned to the coding region were used for
533 further analysis.
534 To infer the ribosome A-site position, python package Plastid[48] was used to align the 3' end
535 of reads to the stop and start codons[49], which are known to have higher ribosome densities. We
536 found that the offsets were 12 nt for stop codon and 15 nt for start codon. Therefore, we used
537 11nt for A site position and 14nt for P site. The counts were normalized to the total counts in the
538 coding region as reads per million (RPM) and transcripts per million (TPM). Further analysis
539 was done using customized Python and R codes with packages including Plastid, dplyr, tidyr
540 and ggplot2.
541
542 Analysis of ribosome profiling data
543 Transcripts per million (TPM) was used to identify highly expressed genes for codon
544 occupancy analysis. After assigning each mapped read to the A-site nucleotide, the raw counts
545 were first normalized by the length of their mapped coding region, to yield count density for each
546 gene. These count densities were then globally normalized to one million counts across all
547 genes within one sample. To determine codon occupancy, transcripts having total counts over
548 100 TPM and containing more than 200 codons were considered. Ribosome footprint counts for
549 the first and last 40 codons were removed to avoid possible effects from initiation and
550 termination, and counts per codon were recorded for the remaining counts. For each gene and
551 each codon type, the codon occupancy ratio is defined as the ratio of measured counts to
552 expected counts. Expected counts are simply proportional to the frequency of that particular
553 codon in the gene. The final reported codon occupancy ratio is the average of codon occupancy
554 ratios from all genes considered weighted equally.
555 We calculated ribosome counts along a transcript using reads per million (RPM). Only
556 transcripts having total counts over 10 TPM and containing more than 100 codons were
557 considered. Total counts after filtering were normalized to one million reads. The selected genes
558 account for more than 85% of the total counts. The ribosome counts are the sum of RPM at
559 each position.
560 To do the first and second halves comparison of ribosome counts of genes, the same set
561 of genes and trimming processing for codon occupancy were used. The RPM from positions
562 were summed up based on its assigned location (first or second half) on the transcript and plot
563 against each other.
564

565 Code availability

566 All the codes used for data analysis in this paper are available upon request.

567 Data availability

568 All the data used to reach the conclusion of this paper will be made available upon publication
569 on SRA BioProject with submission number SUB3256640.

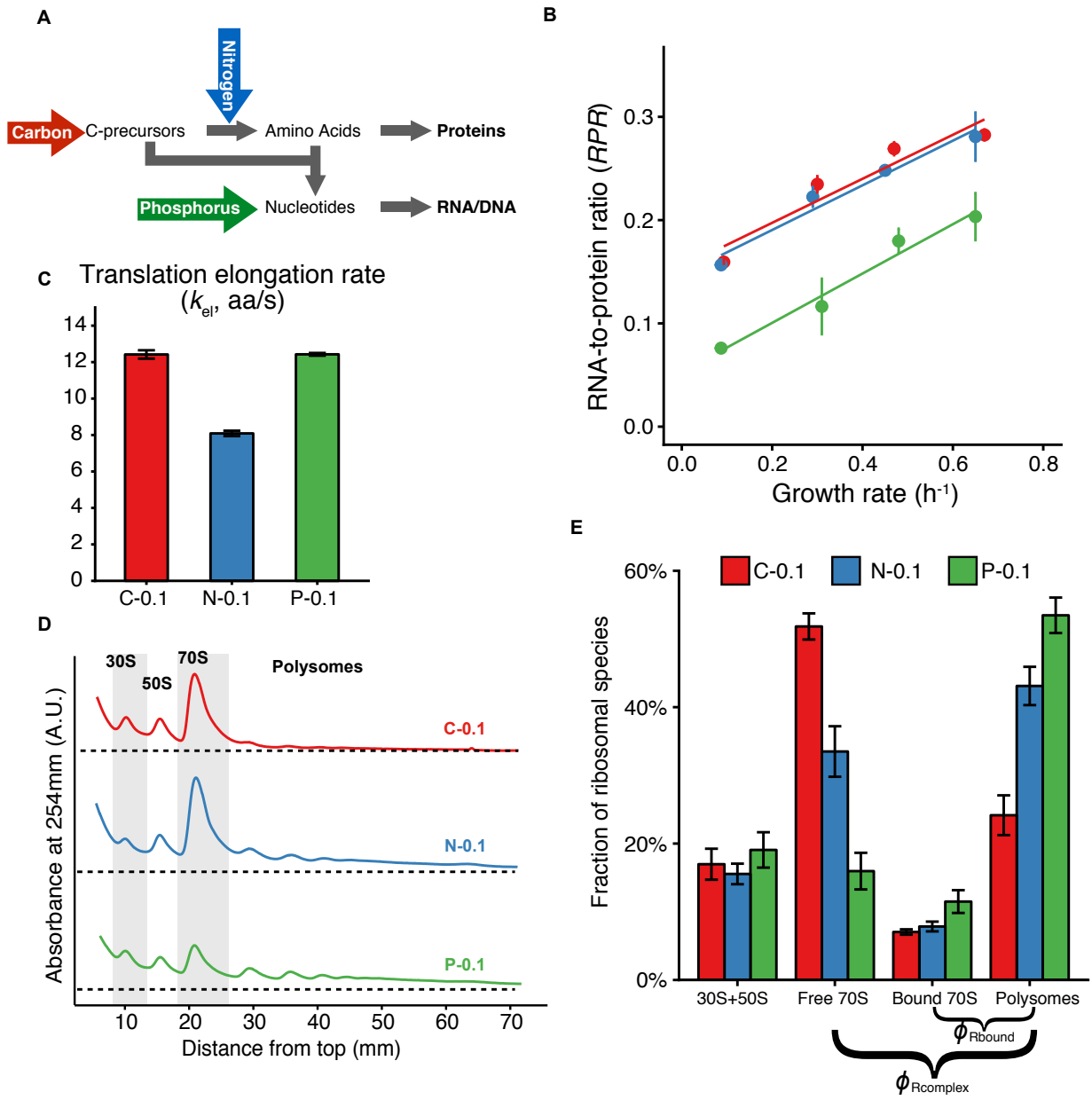

F

Sample	*RPR*	$\phi_{Rcomplex}$	ϕ_{Rbound}	k_{el} (aa/s)	Estimated growth rate from all 70S(h^{-1})	Estimated growth rate from bound 70S (h^{-1})	Actual growth rate (h^{-1})
C-0.1	0.16 ±0.00	0.83 ±0.02	0.31 ±0.03	12.4 ±0.2	0.32±0.0	0.12±0.0	0.09±0.00
N-0.1	0.16 ±0.00	0.84 ±0.02	0.51 ±0.03	8.1 ±0.1	0.21±0.0	0.13±0.0	0.09±0.00
P-0.1	0.08 ±0.00	0.81 ±0.03	0.65 ±0.04	12.4 ±0.1	0.15±0.0	0.12±0.0	0.09±0.01

Figure 1. RNA-to-protein ratio is both growth-rate and nutrient dependent. (A) Schematic flow of nutrients for biomass formation. Carbon (C) and nitrogen (N) combine to make amino acids. Amino acids combine with carbon precursors and phosphorus (P) to make nucleic acids. **(B)** RNA-to-protein ratio for chemostat cultures upon C-, N-, and P-limitations at different growth rates. Each data point represents three technical replicates with standard deviations after error propagation shown as error bars. (See also Figure S1.) **(C)** Translation elongation rates (amino acids/s) as measured by the *lacZ* induction assay after correction for translation initiation. Error bars show the standard error from three biological replicates. **(D)** Polysome profiles of cells grown in C-, N-, P-limitations in chemostats at dilution rate 0.1 h^{-1}. **(E)** Quantification of ribosomes in the form of subunits (30S + 50S), free 70S, mRNA-bound 70S (one ribosome on one mRNA), and polysomes (multiple ribosomes on one mRNA). Three biological replicates were analyzed with the error bars showing standard error of the mean. **(F)** Estimation of growth rate using measurements from RNA-to-protein ratio, elongation rates, and fractions of different ribosomal species.

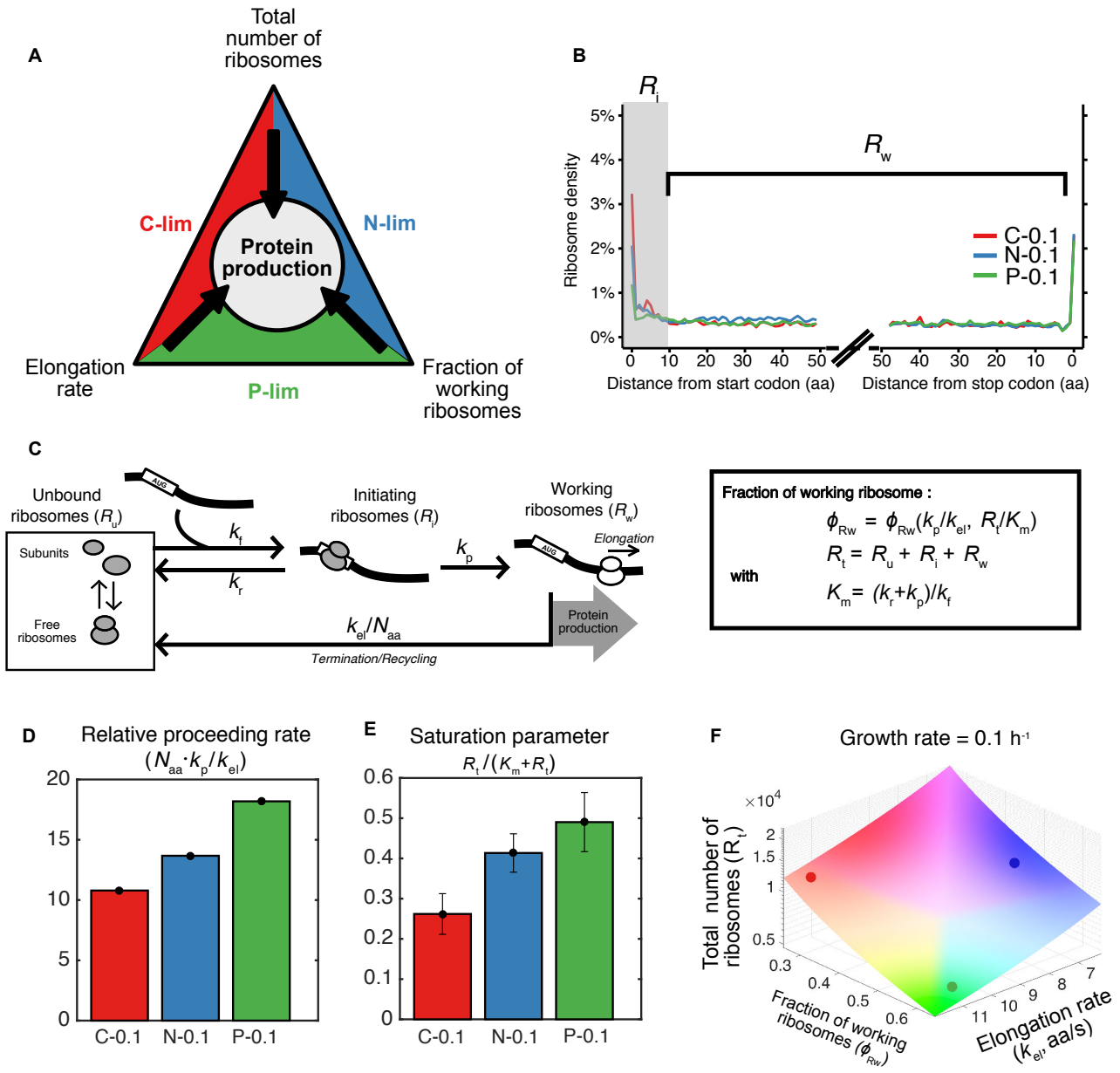

Figure 2. Macroscopic model reveals different ribosome dynamics that achieve the same growth rate. **(A)** Cells adapt to different nutrient limitations using different strategies of translational regulation that achieve the same protein production rate. **(B)** Averaged A-site ribosome counts within the first and last 50 codons of transcripts from ribosome profiling analysis. Ribosomes bound to the first 10 codons are defined as "initiating ribosomes" (R_i) and those bound to the rest of transcripts except the stop codon are "working ribosomes" (R_w). **(C)** Macroscopic model of ribosome dynamics. k_f forward rate (s^{-1}); k_p proceeding rate (s^{-1}); k_{el} elongation rate (aa/s); N_{aa} number of amino acids in an average protein of *E. coli*; k_r aborted translation rate (s^{-1}); R_t total number of ribosomes. **(D)** The relative proceeding rate under C-,N-,P-limitations at growth rate 0.1 h^{-1}. **(E)** The saturation parameter under C-,N-,P-limitations at growth rate 0.1 h^{-1}. **(F)** The relationship between elongation rate (k_{el}), fraction of working ribosomes (ϕ_{Rw}) and total number of ribosomes (R_t) that leads to the same growth rate at 0.1 h^{-1}. Colored dots indicate the values for C-, N-, P-limited wild type cells.

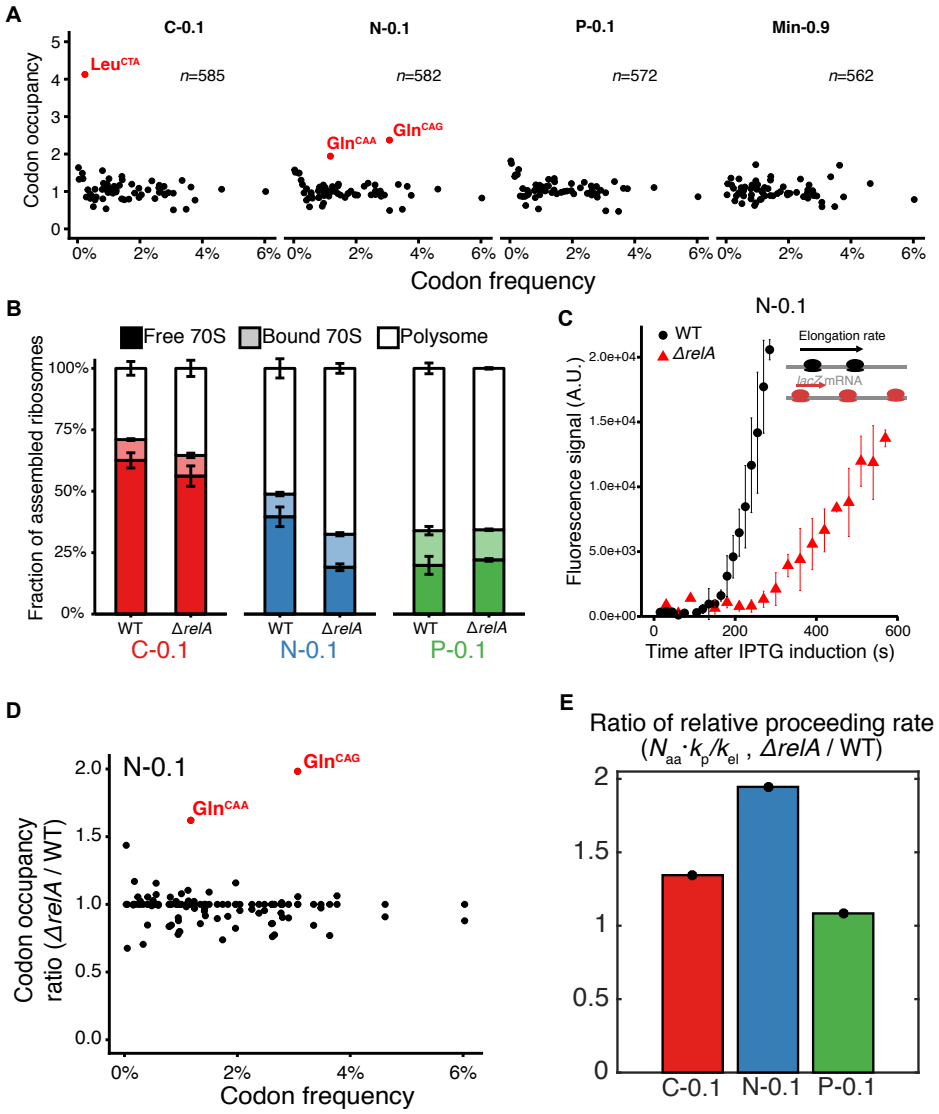

Figure 3. Deletion of *relA* disrupts translation regulation under nitrogen limitation. (A) A-site codon occupancy under different growth conditions from ribosome profiling. Occupancy was calculated as the ratio between measured and expected counts for each gene based on codon frequency. The average of this ratio is plotted (with number of genes specified). Codons that have higher than average ratio by 2.5 standard deviations are highlighted. **(B)** Fraction of assembled (70S) ribosomes in wild type and Δ*relA* under C-, N-, and P-limitation at growth rate 0.1 h^{-1}. Error bars show the standard error from three biological replicates. **(C)** *lacZ* induction assay for wild type and Δ*relA* under nitrogen limitation at growth rate 0.1 h^{-1}. The lag time measures when the first functional LacZ is produced and is inversely proportional to the elongation rate. The error bars show standard error from three biological replicates at each time point. **(D)** Ratio of codon occupancy between Δ*relA* and wild type under nitrogen limitation at growth rate 0.1 h^{-1}. **(E)** Ratio of the relative proceeding rate ($N_{aa} \cdot k_p/k_{el}$) between Δ*relA* and wild type across different conditions at growth rate 0.1 h^{-1}.

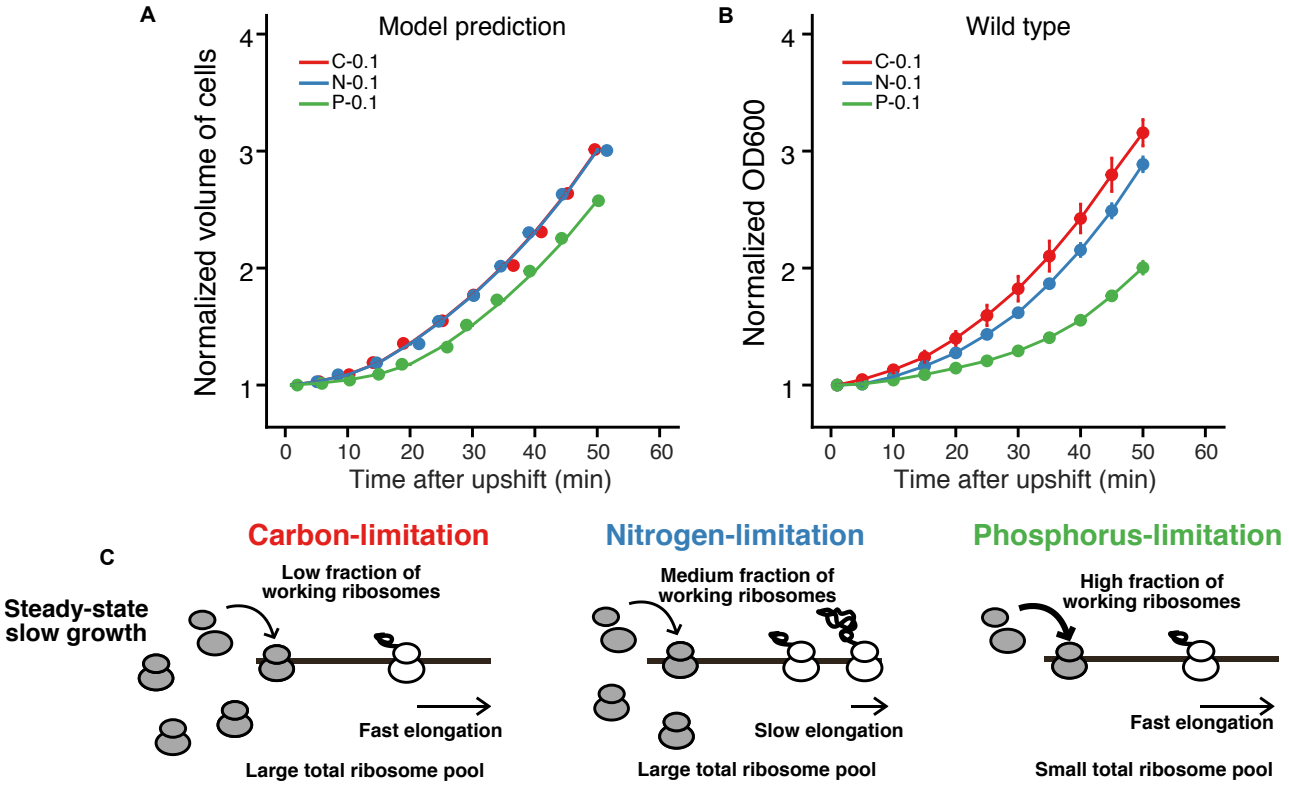

Figure 4. Extra ribosomes confer growth advantage upon nutrient upshift. (A) Theoretically predicted growth curves from the macroscopic model. **(B)** Experimental nutrient-upshift growth curves in LB + 0.4% glucose for wild type cells from C-, N-, and P-limited chemostats at growth rate 0.1 h^{-1}. **(C)** Model for nutrient-dependent ribosome usage: Under C- or N-limitation, the total ribosome pool is high while under P-limitation the total pool is low. C-limited cells elongate fast but have a low fraction of working ribosomes. N-limited cells elongate slower but have a higher fraction of working ribosomes than C-limited cells. Under P-limitation the low supply of ribosomes leads to both a high fraction of working ribosomes and fast elongation to meet the protein production demand.